Journal of Applied Electrochemistry (2021) 51:1111–1122
https://doi.org/10.1007/s10800-021-01562-0

RESEARCH ARTICLE

The effect of TEOS concentration in polysulphide electrolyte and CuS counter electrode on enhancing the performance of CdS quantum dot sensitized solar cells

T. Archana[1] · G. Subashini[2] · A. Nirmala Grace[2] · M. Arivanandhan[1] · R. Jayavel[1]

Received: 28 October 2020 / Accepted: 10 March 2021 / Published online: 29 March 2021

Abstract

Titanium dioxide photoanode and copper sulphide photocathode were prepared by optimizing the conditions. Cadmium sulphide quantum dots were loaded onto the photoanode by successive ionic layer adsorption and reaction method. The effective loading of CdS QDs onto TiO_2 photoanodes was confirmed by XRD, SEM and optical studies. Copper sulphide counter electrodes were prepared by two different methods. Quantum dot-sensitized solar cells (QDSSCs) were fabricated by sandwiching the cadmium sulphide quantum dots loaded photoanode and copper sulphide counter electrodes. The *J–V* characteristics of CdS-based QDSSC with optimum photoanode along with passivating layer were studied by adding different vol% of TEOS into polysulphide electrolyte. The efficiency of QDSSC with copper sulphide counter electrodes was relatively enhanced compared to the cell with platinum counter electrodes. Furthermore, QDSSC with copper sulphide counter electrodes and 2.5 vol% TEOS-modified electrolyte exhibited high efficiency of 5.5% which offered 0.543 V open circuit voltage and 19.33 mA cm^{-2} short circuit current density with a fill factor value of 0.523. The mechanism for improving the efficiency of QDSSC is discussed based on electrochemical impedance spectroscopy.

Graphical abstract

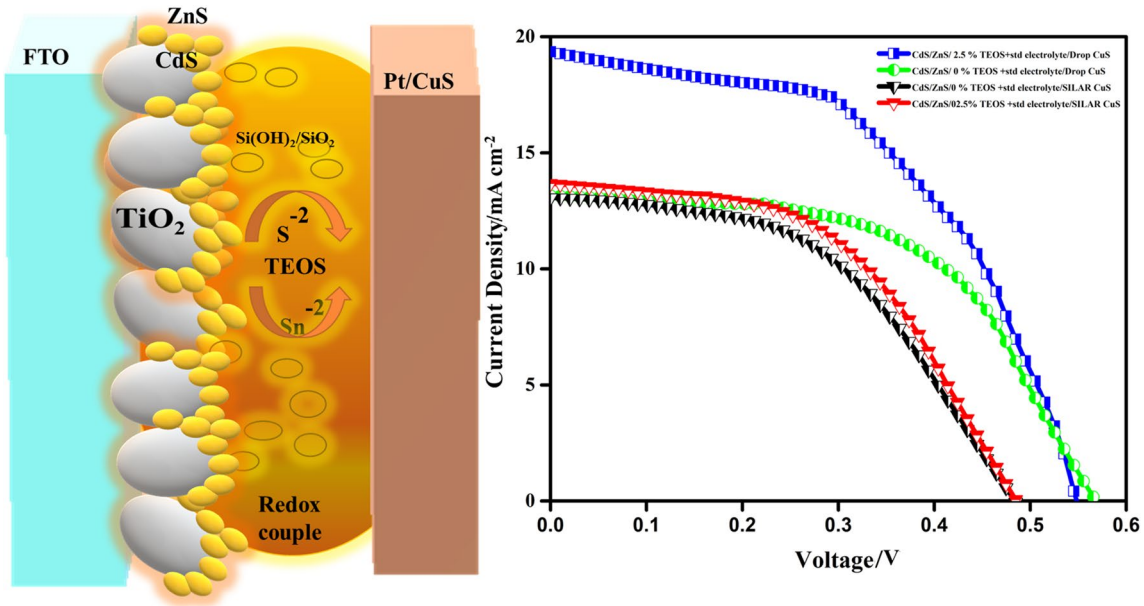

Keywords Quantum dot · Passivation · Photocurrent density · Recombination losses · Polysulphide electrolyte

Extended author information available on the last page of the article

1 Introduction

Quantum Dots (QDs) exhibit tunable bandgap, high optical absorption coefficient, solution processability, photostability, high molar extinction coefficient which leads to broadened application in photonics, bioimaging and solar cells [1]. QDs as sensitizer for quantum dot-sensitized solar cells (QDSSCs) showed a possibility to achieve higher conversion efficiency than that of Si solar cells by overcoming Shockley Queisser effect [2]. On the contrary, the progress of QDSSC was slow down due to poor stability of dye molecules, high corrosive nature of electrolytes, recombination losses and other interface losses [3]. Therefore, it is highly essential to improve the performance of QDSSC by optimizing the photoanode, QD sensitizer, redox electrolyte and counter electrode (CE) [4].

Polysulphide is a widely used electrolyte for QDSSC. However, the main issue with polysulphide electrolyte is its high regeneration rate of oxidized QDs that leads to lower open circuit voltage (V_{oc}) [5]. Moreover, low interfacial recombination resistance at CE/electrolyte interface affects the charge transfer which in turn degrade the cell performance. Hence various strategies have been tried to modify the standard polysulphide electrolyte in QDSSC [6]. Yu et al. reported photovoltaic characteristics of polyacrylamide-based hydrogel-modified CdS/CdSe co-sensitized QDSSC. They have reported relatively high efficiency of 4% that resulted from high ionic conductivity of quasi hydrogel electrolyte [7]. Recently, Du et al. enhanced the efficiency of CdSe-based QDSSC from 5.8 to 6.74% by modifying the polysulphide electrolyte using polyethylene glycol (PEG) which reduced the charge recombination occurring at the TiO_2/QDs/electrolyte interfaces [8]. Yu et al. reported the modification of polysulphide electrolyte using TEOS as additive and studied the effect of tetraethyl orthosilicate (TEOS) addition in Zn–Cu–In–Se, CdSeTe and CdSe-based QDSSC systems [9]. However, the effect of TEOS addition in polysulphide electrolyte has not yet been investigated in the CdS QDs-based QDSSC. Therefore, in the present work, polysulphide electrolyte has been modified by adding TEOS to study its effect on the performance of CdS-based QDSSCs.

As an energetic component, CE is also significantly influencing on photovoltaic performance of QDSSC as that of photoanode [10], sensitizer and electrolyte. Platinum (Pt) is widely used as CE for QDSSC despite of its high cost. Different kind of materials such as CoS, CuS and NiS [11–14] and NiS_2 [15] have been tried as CE for replacing Pt in QDSSCs. Xu et al. reported FeS_2 microspheres-based CE for QDSSCs [16]. From the recent literatures, it is obvious that the Cu-based chalcogenides are the promising CEs for QDSSC [17–19]. Therefore, in the present work, the Pt CE has been replaced by CuS along with electrolyte modification for possible improvement in the overall performance of QDSSC. The photoanodes and CEs were prepared by optimizing the conditions. The QDSSCs were fabricated by sandwiching the CdS QDs loaded TiO_2 photoanode and CuS CE. The TEOS-modified polysulphide electrolyte with different concentrations have been filled into the cell and comparatively studied its performance to determine the optimum TEOS concentration in polysulphide electrolyte for enhancing QDSSC performance. The QDSSC with 2.5 vol % TEOS added polysulphide electrolyte and modified CuS CE shows the high efficiency of 5.5%.

2 Materials and methods

Titanium tetraisopropoxide (TTIP), fluorine doped tin oxide (FTO) (7 Ω resistance), tetraethyl orthosilicate (TEOS), chloroplatinic acid (H_2PtCl_6), sulphur (S) (Sigma Aldrich), acetic acid, cadmium chloride ($CdCl_2$), copper nitrate ($Cu(NO_3)_2$), methanol, acetone, nitric acid (HNO_3) (Alfa Aesar) sodium sulphide (Na_2S), α-terpineol, potassium chloride (KCl), zinc acetate ($Zn(OAc)_2$), ethyl cellulose (TCI chemicals) ethanol (Honeywell) were used as received without any further purification.

2.1 Preparation of TiO_2-coated photoanode

FTO substrates were sonicated initially with soap solution for 10 min followed by treatment with double distilled water and ethanol for further purification. Finally, the cleaned substrates were dried at air. TiO_2 nanoparticles were prepared by hydrothermal method using TTIP as precursor in Teflon-lined autoclave at 240 ℃ for 12 h [18]. As prepared TiO_2 nanoparticles were washed using double distilled water, centrifuged at 6000 rpm and finally dried at 100 ℃. TiO_2 paste was prepared by grinding TiO_2 nanoparticles with specific ratio of acetic acid, double distilled water and ethanol using mortar and pestle. Ethyl cellulose and α-terpineol were added to the above mixture as binders to make a thick paste. The paste was coated over conducting side of FTO substrate which was masked by scotch tape for a coating area of 0.16 cm^2 to make a thin film by doctor blade technique [19]. TiO_2 film was dried at 100 ℃ for 15 min followed by calcination at 450 ℃ for 15 min in a muffle furnace and subsequently cool down to ambient temperature.

2.2 CdS QDs loading

TiO_2 photoanodes were immersed in anionic and cationic precursor of $CdCl_2$ and Na_2S in methanol and water (1:1) mixed solution, followed by purging N_2 gas. Anionic and

cationic precursor solutions were prepared at different concentrations (0.02 M, 0.04 M and 0.06 M) to study the effect of precursor concentrations on QD formation. CdS QDs were loaded on to TiO_2 photoanode with different precursor concentrations by successive ionic layer adsorption and reaction method (SILAR) method at 3, 6 and 9 numbers of deposition cycles. Soaking time for each SILAR cycle was 30 s and the deposition was carried at ambient temperature (~ 32 ℃). Eventually, the QD loaded photoanodes were dried by purging nitrogen gas for 5 min. The CdS QDs loaded TiO_2 photoanodes with different precursor concentrations and cycle of depositions were named as C1 to C9. The CdS QDs loaded TiO_2 photoanodes prepared using 0.02 M precursor concentration with 3, 6 and 9 SILAR cycles of deposition were named as C1, C2 and C3, respectively. The photoanodes prepared using 0.04 M precursor concentration with 3, 6 and 9 SILAR cycles were named as C4, C5 and C6, respectively. The CdS QDs loaded prepared for 0.06 M precursor concentration with 3, 6 and 9 SILAR cycles were named as C7, C8 and C9, respectively. ZnS passivation on to CdS QDs loaded TiO_2 photoanode was carried out by soaking the electrodes into 0.1 M Zinc acetate solution and 0.1 M Na_2S solution. The optimal immersion time was 60 s for both solutions [20, 21].

2.3 Preparation of modified electrolyte

Standard polysulphide electrolyte solution was prepared by mixing 0.5 M Na_2S, 1 M S, and 0.2 M KCl and ground thoroughly using a mortar and pestle before introduced into the solution media. The mixture of water and methanol (7:3 volume ratio) was used as a solvent medium [3, 5–7]. The polysulphide electrolyte was modified by adding different volume % of TEOS (1, 1.5, 2, 2.5, 3 and 3.5 vol%) into the solution to study the effect of TEOS concentration on the performance of QDSSC.

2.4 Preparation of CE

Doctor blade method was used for preparing Pt CE, by depositing a thin layer of 20 mM H_2PtCl_6 on the conducting side of well cleaned FTO substrate followed by thermal treatment at 450 ℃ for a duration of 30 min [8–10]. CuS CEs were prepared by SILAR and drop casting methods for comparative analysis. CuS CE was prepared by SILAR deposition of 1 M Cu $(NO_3)_2$ and Na_2S in methanol, with 8 cycles. CuS-coated substrates were dried at 80 ℃ for 60 min [22]. For CuS coating by drop casting, 100 µL of 0.5 M Cu $(NO_3)_2$ in methanol solution was dropped on to FTO. 100 µL of Na_2S in mixture of water and methanol (3:7) was dropped over the initial layer. CuS formation was confirmed by the change of colour from blue to brown and finally to black. This procedure was repeated for three times followed by rinsing with ethanol. The films were dried at 120 ℃ for 60 min [23–26].

2.5 QDSSC fabrication

QDSSCs were fabricated by sandwiching the CdS QDs loaded TiO_2 photoanodes and Pt/CuS CEs using binder clips. The space between electrodes was separated by parafilm of 60 µm thickness. The TEOS-modified polysulphide electrolyte was loaded into sandwiched cell region of two electrodes through capillary action. The cells were fabricated with different configurations for optimizing the cell structure to achieve high performance.

3 Results and discussion

Figure 1 shows UV-DRS spectra of CdS QDs loaded TiO_2 photoanodes prepared with different precursor concentrations and different numbers of SILAR cycles (C1 to C9). The optical spectra of C1, C2, C3 samples show that the reflectance onset increased from 450 to 500 nm, when SILAR cycles increased from 3 to 9 at same precursor concentration of 0.02 M resulted low optical reflectance with SILAR cycles. Similar effect is observed for the other precursor concentrations of 0.04 and 0.06 M. From the DRS analysis, an obvious shift towards visible region is observed when the number of SILAR cycles increased to 9 at all precursor concentrations which confirms the effective loading of CdS QDs on TiO_2 photoanode. Moreover, low reflectivity can be seen in the samples with 9 SILAR cycles due to high absorption by QDs. In particular, maximum red shift is observed for C9 photoanode with 0.06 M of precursor concentration

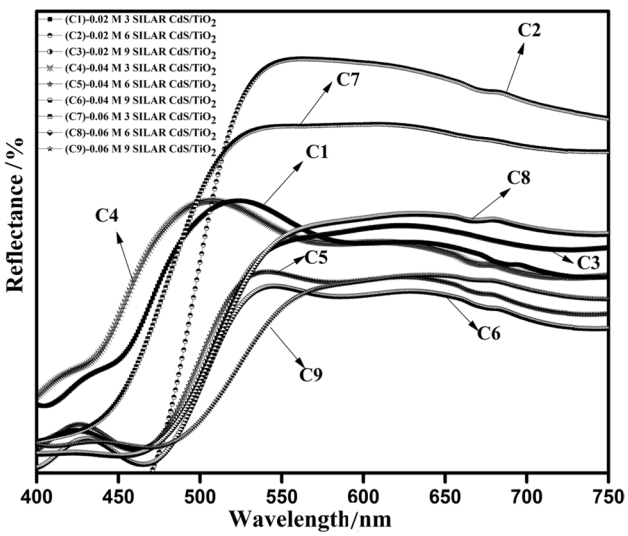

Fig. 1 UV-DRS spectra of CdS QDs loaded TiO_2 photoanodes

and 9 SILAR cycles. Therefore, C9 photoanode has been used for further analysis.

Figure 2a(i, ii, iii) shows the SEM images of C7, C8 and C9 samples. TiO_2 with larger grain size can be seen from the SEM image of C7 in Fig. 2a(i) which shows that CdS QDs are not completely covered on the photoanode surface. However, the SEM image of C9 samples from Fig. 2a(iii) shows the complete coverage of ultra-small size CdS QDs on the TiO_2 photoanode surface due to the effective loading of QDs after 9 SILAR cycles of QD deposition. SEM images further confirm that C9 is an optimized photoanode for fabrication of QDSSCs and therefore further analysis is carried out for C9 photoanode. Figure 2b(i and ii) shows FESEM images of CuS CEs prepared by SILAR and DROP casting method. Rod like morphology is obtained for the SILAR deposited CE, whereas flower-like morphology is observed

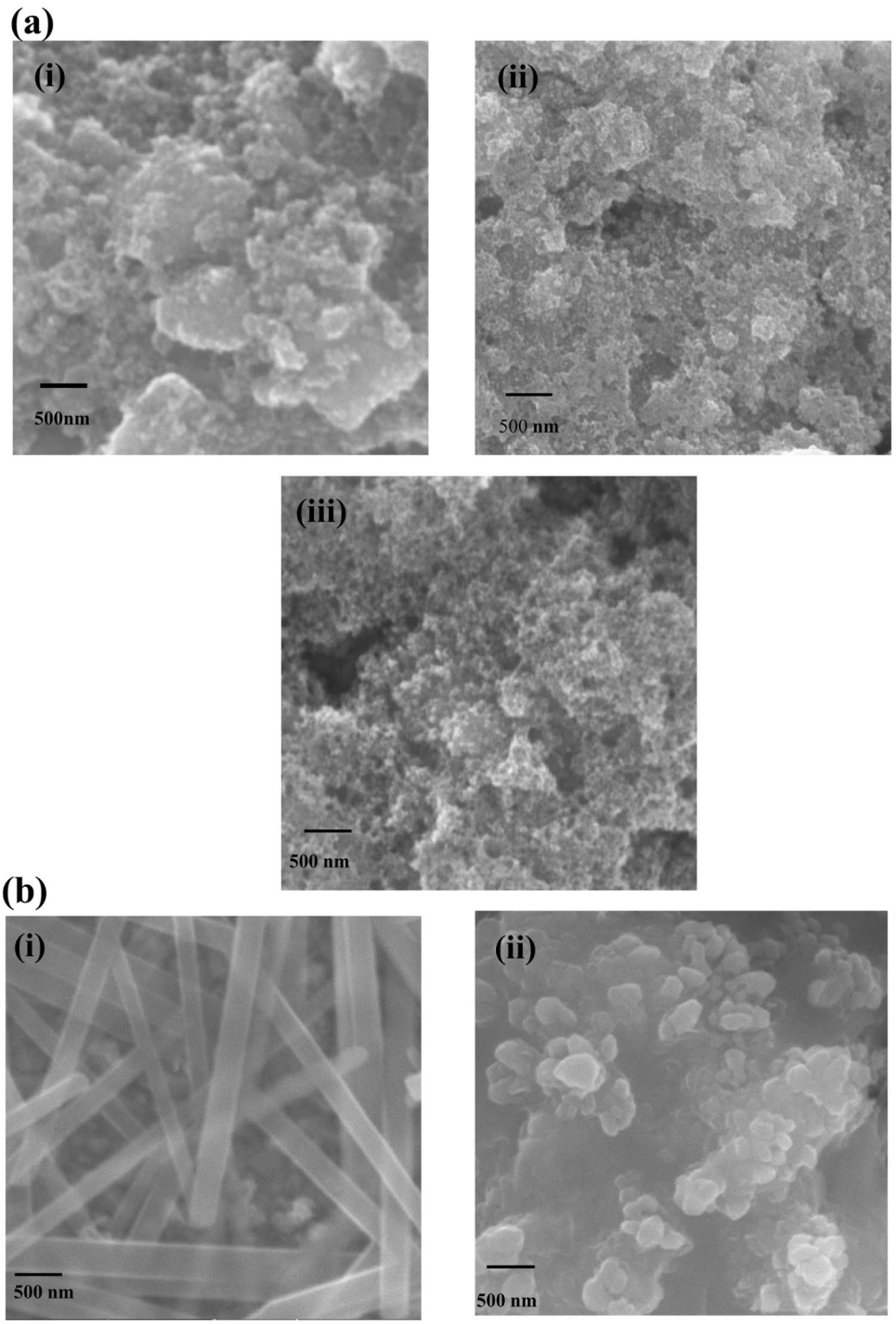

Fig. 2 FESEM images of (**a**) CdS QDs loaded photoanodes **i** C7, **ii** C8, **iii** C9; (**b**) CuS CE **i** SILAR, **ii** Drop casting

for drop-casted CuS CE. Figure 3a, b shows the high-resolution SEM images of CdS loaded photoanode (C9) with ZnS passivation. The top view of SEM image shows the homogeneous distribution of CdS QDs on the surface of photoanode. Figure 3c shows the EDAX spectrum of ZnS passivated CdS QDs loaded photoanode which confirms the presence ZnS over CdS loaded TiO_2 photoanode.

To evaluate the effect of ZnS passivation, the photoluminescence (PL) spectra are recorded for bare TiO_2 and CdS QDs loaded photoanodes at different excitation wavelength of 350, 380 and 400 nm and shown in Fig. 4a–c. In general, the PL emission is the result of recombination of photogenerated electrons and holes. Hence, a weak emission is an evidence of decreased charge recombination with longer excitonic lifetime of the carriers [10]. From Fig. 4a–c, the PL emission for bare TiO_2 photoanodes, CdS QDs loaded TiO_2 photoanodes (C7, C8 and C9) and ZnS passivated C9 photoanode are observed around 550 nm. The emission peaks related to CdS QDs are observed in the PL spectra for the excitation wavelength of 380 and 400 nm (Fig. 4a), whereas those peaks are not observed in the spectra with excitation wavelength of 350 nm. The inset in Fig. 4b clearly shows the CdS QDs-related emission peaks in the visible region and the intensity of the peak varied with number of SILAR cycles [27]. Moreover, the peaks are relatively shifted towards lower wavelength in the ZnS passivated photoanodes due to wide bandgap of ZnS, which confirms its effective passivation on the QDs surface (Fig. 4c).

Figure 5 shows the Raman spectra of ZnS passivated and unpassivated CdS QDs loaded photoanodes (C9). Peaks observed at 146, 398, 517 and 638 cm^{-1} confirm the anatase phase of TiO_2 photoanode material [10]. A low intensity peak was observed at 330 cm^{-1} related to CdS which is slightly shifted in the ZnS passivated sample. Additionally,

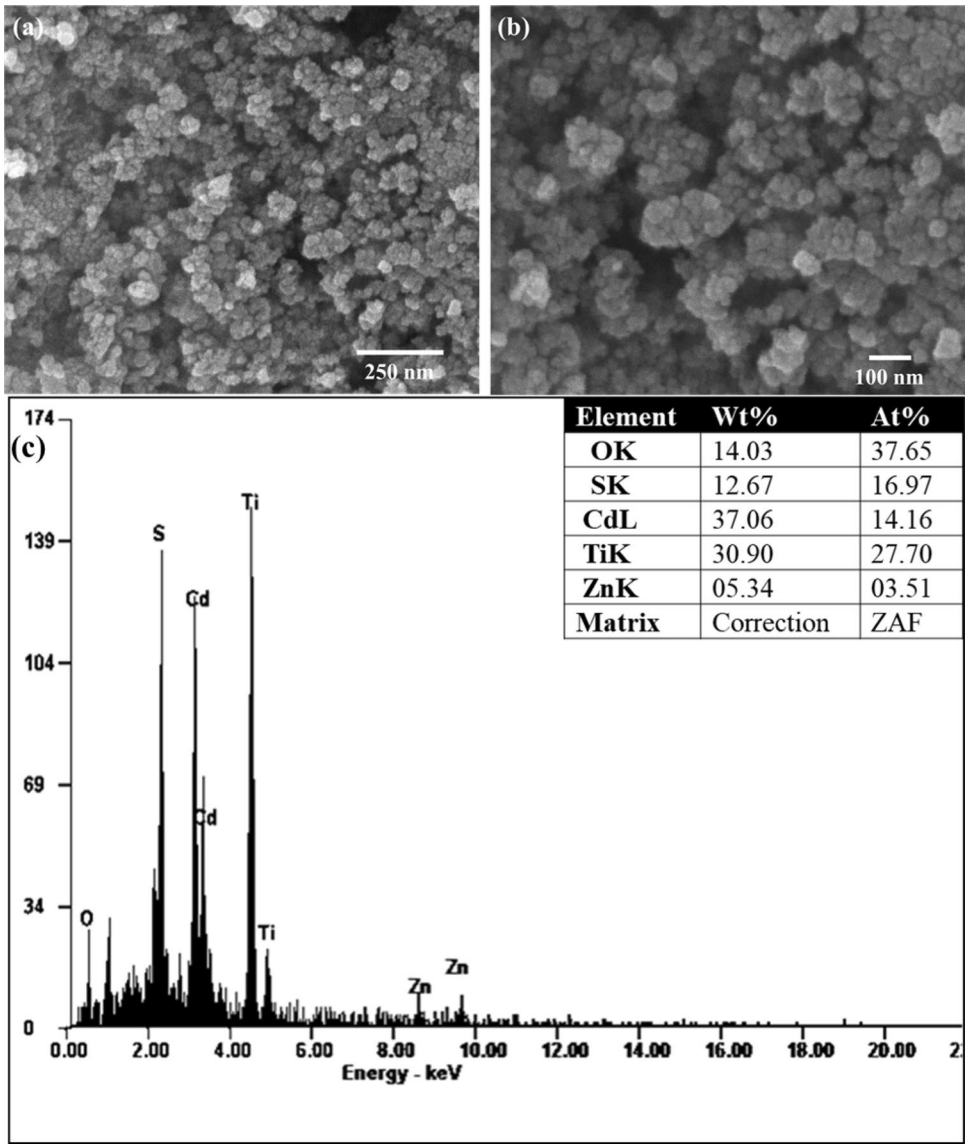

Element	Wt%	At%
OK	14.03	37.65
SK	12.67	16.97
CdL	37.06	14.16
TiK	30.90	27.70
ZnK	05.34	03.51
Matrix	Correction	ZAF

Fig. 3 Top view of FESEM images (**a** and **b**) and Energy dispersive X-ray spectra (**c**) of CdS loaded TiO_2 photoanodes C9 with ZnS passivation layer

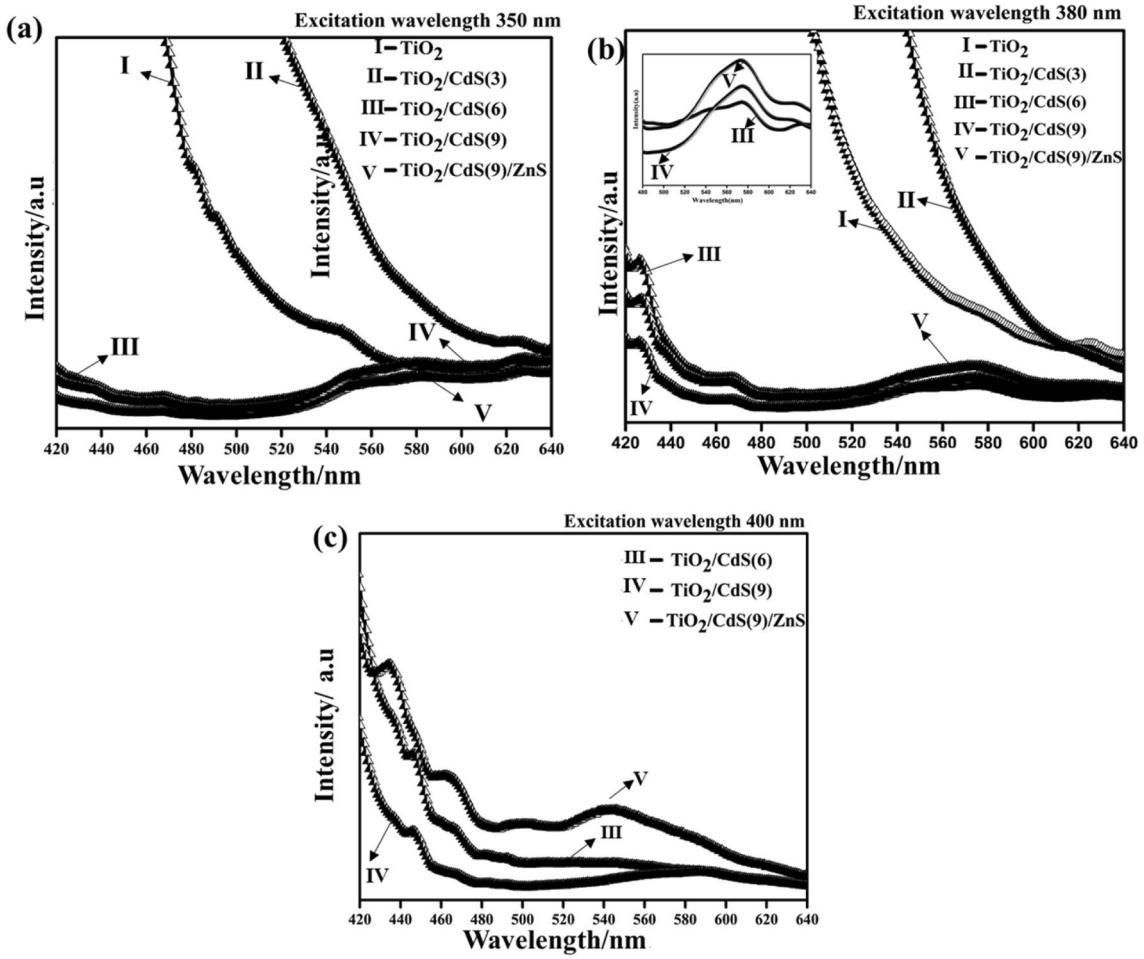

Fig. 4 Photoluminescence spectra at an excitation wavelength: (**a**) 350 nm (**b**) 380 nm (**c**) 400 nm for TiO_2, C7, C8, C9, ZnS passivated C9 photoanodes

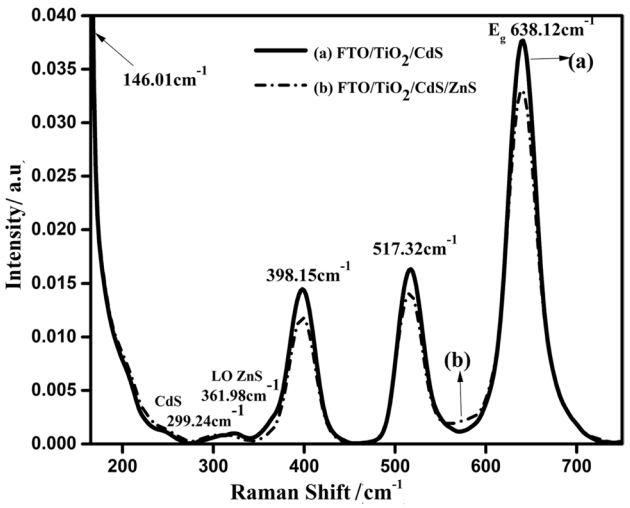

Fig. 5 Raman spectra of (**a**) unpassivated and (**b**) ZnS passivated CdS (C9) loaded TiO_2 photoanodes

the intensity of the Raman peaks decreased for the ZnS passivated CdS loaded photoanode compared to that of unpassivated photoanode.

Figure 6a and b shows the X-ray diffraction patterns of ZnS passivated and unpassivated CdS loaded TiO_2 photoanodes (C9). The diffraction peaks of TiO_2 matches with JCPDS card no: 21-1272 which confirms the anatase phase of TiO_2 and CdS-related diffraction peaks are well matched with JCPDS card no: 10-454. Additionally, ZnS peaks can be observed for photoanode with passivation (Fig. 6a) which confirms effective passivation of ZnS on CdS loaded photoanode [27, 28]. Figure 6c and d shows the X-ray diffraction patterns of CE of CuS on FTO substrate prepared by SILAR and drop casting method. The diffraction peaks correspond to hexagonal CuS are well matched with JCPDS card no. 79-2321 [26]. Further, the diffraction peaks related to FTO substrate are also observed for both photoanodes and CEs.

Figure 7a shows the *J*–*V* curves of QDSSCs fabricated using modified electrolyte with different vol% of TEOS and

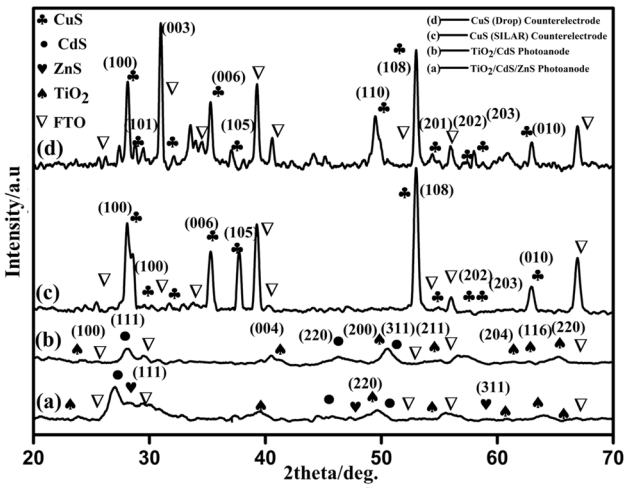

Fig. 6 XRD diffraction patterns of (**a**) ZnS passivated C9, (**b**) C9, (**c**) SILAR deposited CuS on FTO, (**d**) CuS deposited by drop casting on FTO

Pt CE. From the *J–V* curves, various photovoltaic parameters (photoconversion efficiency (PCE), Fill factor (FF), open circuit voltage (V_{oc}) and short circuit current density (J_{sc})) are extracted and tabulated in Table 1. From the *J–V* curves, it is found that the efficiency of QDSSC increased to 1.8% when TEOS vol% increased up to 2.5% in electrolyte. Figure 7b shows the variation of V_{oc} and J_{sc} of QDSSC as a function of TEOS concentration in the modified electrolyte. Both J_{sc} and V_{oc} of QDSSC increased reasonably with increase of TEOS content in the polysulphide electrolyte and approached the peak values for 2.5 vol% of TEOS. When the TEOS content increased beyond 2.5 vol%, J_{sc} and V_{oc} are started to decline gradually and thereby the efficiency of cells decreased. Figure 7c shows the variation of PCE and FF of QDSSC as a function of TEOS concentration in the modified electrolyte. At higher concentration of TEOS, silicates are accumulated in the electrolyte which affected the redox potential thereby J_{sc} and PCE decreased [9]. From *J–V* analysis, 2.5 vol% of TEOS is considered as an optimum concentration for modifying the standard polysulphide electrolyte and used the same for further study. To study the role of TEOS in the performance of QDSSC operation, *J–V* and EIS analyses were performed for CdS QDSSC without

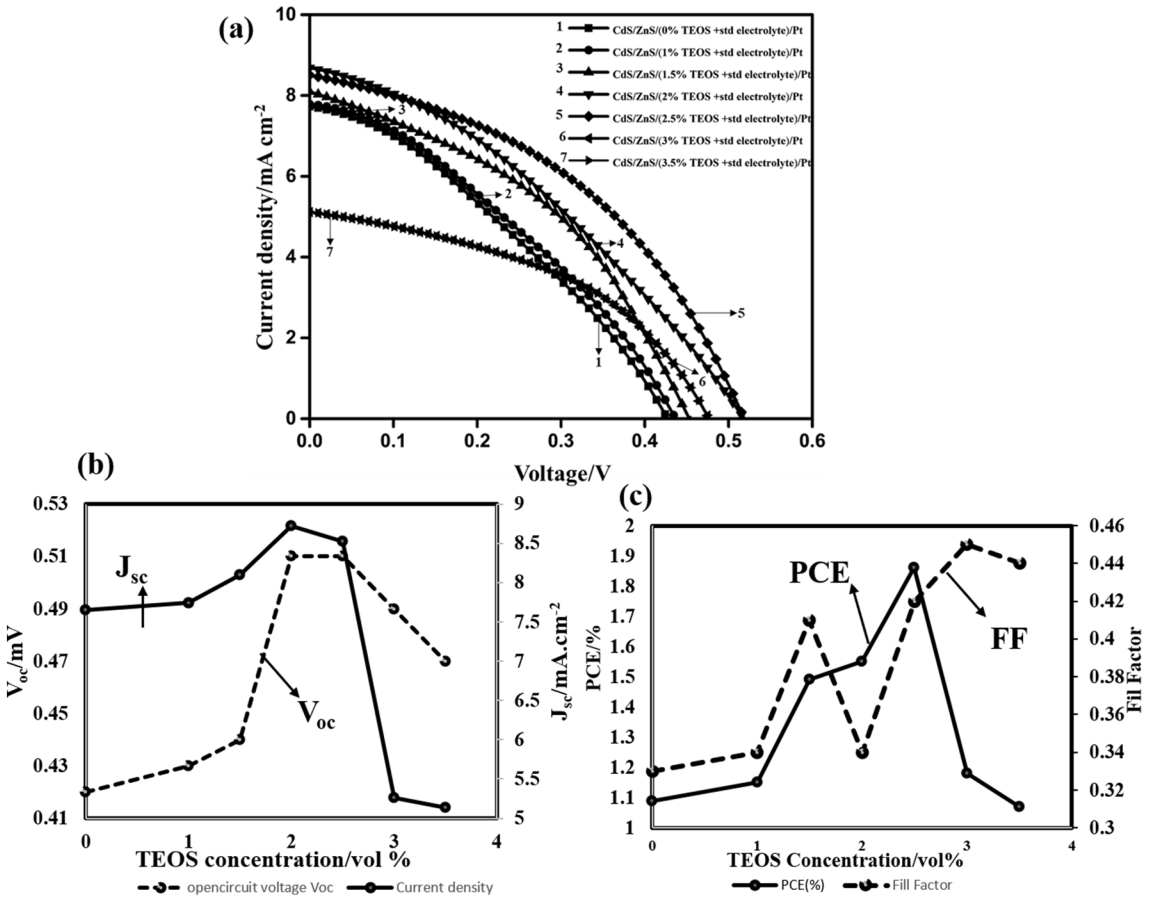

Fig. 7 (**a**) *J–V* curves (**b**) variation of average V_{oc} and J_{sc}, (**c**) variation of PCE and FF of CdS QDSSCs with various concentrations of TEOS in the modified polysulphide electrolyte

Table 1 *J–V* characteristics of QDSSC with different vol% of TEOS added polysulphide electrolyte and Pt CE

Cell configurations	V_{oc} (V)	J_{sc} (mA cm^{-2})	Fill Factor	Efficiency (%)
TiO_2/CdS/ZnS/Es + 0% TEOS/Pt	0.42	7.67	0.335	1.09
TiO_2/CdS/ZnS/Es + 1% TEOS/Pt	0.43	7.74	0.344	1.15
TiO_2/CdS/ZnS/Es + 1.5% TEOS/Pt	0.44	8.10	0.413	1.49
TiO_2/CdS/ZnS/Es + 2% TEOS/Pt	0.51	8.72	0.345	1.55
TiO_2/CdS/ZnS/Es + 2.5% TEOS/Pt	0.51	8.52	0.422	1.86
TiO_2/CdS/ZnS/Es + 3% TEOS/Pt	0.49	5.26	0.454	1.18
TiO_2/CdS/ZnS/Es + 3.5% TEOS/Pt	0.47	5.14	0.439	1.07

Es standard electrolyte

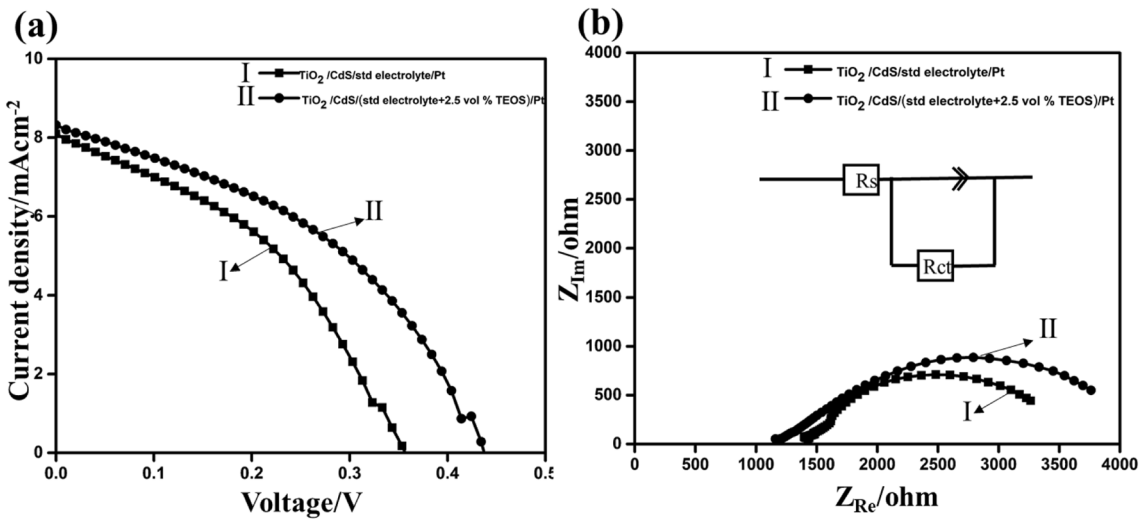

Fig. 8 (**a**) *J–V* characteristics (**b**) EIS spectra, of CdS-based QDSSCs using Pt CE with TEOS-free and TEOS-modified electrolytes (inset of **b** EIS fitting equivalent circuit)

Table 2 *J–V* characteristics and EIS parameters of CdS-based QDSSCs using Pt CE with TEOS-free and TEOS-modified electrolytes

Cell configurations	V_{oc} (V)	J_{sc} (mA cm^{-2})	Fill factor	Efficiency (%)	R_s (Ω)	R_{ct} (Ω)
TiO_2/CdS/Es/Pt	0.358	8.08	0.39	1.14	1407	2923
TiO_2/CdS/Es + 2.5% TEOS/Pt	0.435	8.29	0.41	1.50	1168	4504

Es standard electrolyte

ZnS passivation and shown in Fig. 8a, b and corresponding values are tabulated in Table 2. As can be seen from *J–V* curves, the QDSSC with TEOS-modified electrolyte shows improved performance compared to the cell without TEOS. The addition of TEOS in polysulphide electrolyte resulted the in situ passivation, which improved PCE of QDSSC from 1.1 to 1.5%. From EIS analysis high charge transfer resistance (R_{ct}) is observed for the TEOS-modified electrolyte. From the results, it is confirmed that the addition of TEOS to the electrolyte at an optimum concentration has a positive effect in CdS QDSSC by providing additional passivation. Therefore, 2.5 vol% of TEOS-modified polysulphide electrolyte is identified as a promising electrolyte and used for further studies.

To further improve the PCE, QDSSCs were fabricated by replacing Pt CE with CuS CE. The cells were fabricated using CuS CEs prepared by SILAR and drop casting methods. Moreover, to study the effect of modified electrolytes, the CuS CE-based cells were fabricated with and without TEOS in the electrolyte. Figure 9a shows the *J–V* curves of CuS CE-based QDSSCs with standard electrolyte and 2.5 vol% TEOS-modified electrolytes. The obtained PCE (η), V_{oc}, J_{sc}, and FF are summarized in Table 3. It can be observed from Fig. 9, that all the QDSSCs exhibited relatively higher performance with CuS CE. Moreover, the J_{sc} of

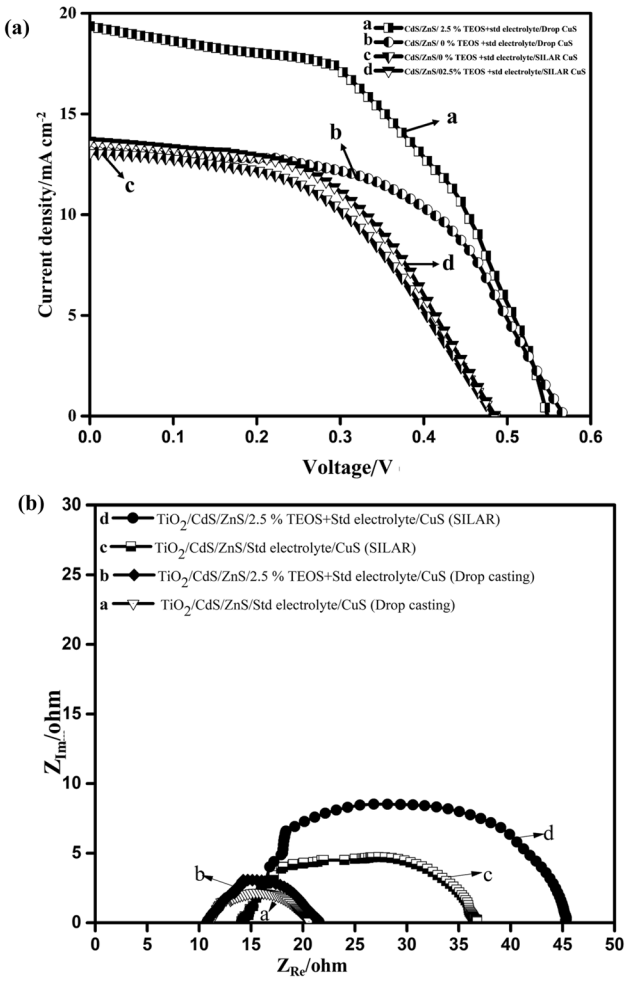

Fig. 9 *J–V* characteristics (**a**) and EIS spectra (**b**) of CdS-based QDSSCs with CuS (SILAR) and CuS (Drop-casted) CEs

the cells are one order increased compared to the cells with Pt as CE (Table 1) which resulted high conversion efficiency. Furthermore, the J_{sc} of cells with drop-casted CuS CE significantly improved compared to the cells with SILAR CuS CE. As a result, the cells with drop-casted CuS CE-based QDSSC with TEOS-modified electrolyte exhibited high efficiency of 5.5% compared to that of SILAR CdS-based QDSSC (3.41%).

Figure 9b shows the EIS spectra of cells with drop-casted CuS and SILAR CuS CEs. From EIS spectra, it is clear that R_{ct} and equivalent series resistance (R_s) of cells with drop-casted CuS CE are relatively lower than that of cells with SILAR CuS CE as the diameter of the semicircle decreased for drop-casted CuS CE-based QDSSCs. Due to low internal resistance, the QDSSC with drop-casted CuS CE shows relatively high efficiency compared to SILAR CuS-based QDSSC [25, 28].

The cell fabricated using drop-casted CuS CE and TEOS-modified electrolyte shows the best performance with V_{oc} 0.543 V, J_{sc} 19.33 mA cm^{-2}, FF 0.523 and PCE of 5.5%. The PCE is far better when compared to the performance of Pt CE-based QDSSC which shows the PCE of 1.86%. The poor performance of QDSSC with Pt CE is mainly attributed to its affinity towards S^{2-} ions which slow down the catalytic activity of Pt and rapidly decreases the charge transfer rate [26]. Due to this fact, Pt has poor reduction rate of S_n^{2-}, resulting in depletion of S^{2-} in the photoanode area and reduces QD regeneration rate. However, the QDSSCs with CuS CEs prepared by both the methods show relatively higher performance due to low R_{ct} and R_s as observed in EIS spectra (Fig. 9b). The excess adsorption of S onto the Pt CE surface by chemisorption leads to a phenomenon called 'catalytic poisoning' resulting in higher resistance [12, 25]. Therefore, electrocatalytic process is limited by the higher internal resistance of Pt which makes CuS as an inevitable alternate CE for QDSSCs.

The EIS analysis of passivation-free QDSSC with TEOS-modified electrolyte and Pt CE throw more light on the role of TEOS in improving the cell performance. Figure 8b shows the Nyquist plots of the symmetric cells with and without TEOS in the frequency range of 0.1 Hz to 500 kHz. As can be seen from Figs. 8b and 9b, the diameter of the semicircle increased for the cell with TEOS-modified electrolyte compared to cell with TEOS-free polysulphide electrolyte. The larger diameter of semicircle refers the higher R_{ct} which results less recombination at the electrolyte/photoanode interfaces

Table 3 *J–V* characteristics and EIS parameters of CdS QDSSC with CuS (SILAR), CuS (Drop-casted) CE with TEOS-free and TEOS-modified electrolytes

Cell configurations	V_{oc} (V)	J_{sc} (mA cm^{-2})	Fill factor	Efficiency (%)	R_s (Ω)	R_{ct} (Ω)
TiO_2/CdS/ZnS/Es/CuS (SILAR)	0.480	13.14	0.488	3.08	16.77	6.44
TiO_2/CdS/ZnS/Es + 2.5% TEOS/CuS (SILAR)	0.480	13.69	0.519	3.41	13.23	10.21
TiO_2/CdS/ZnS/Es/CuS (Drop)	0.537	12.11	0.557	3.62	10.81	9.87
TiO_2/CdS/ZnS/Es + 2.5% TEOS/CuS (Drop)	0.543	19.33	0.523	5.5	9.94	11.97

[#]Es = standard electrolyte

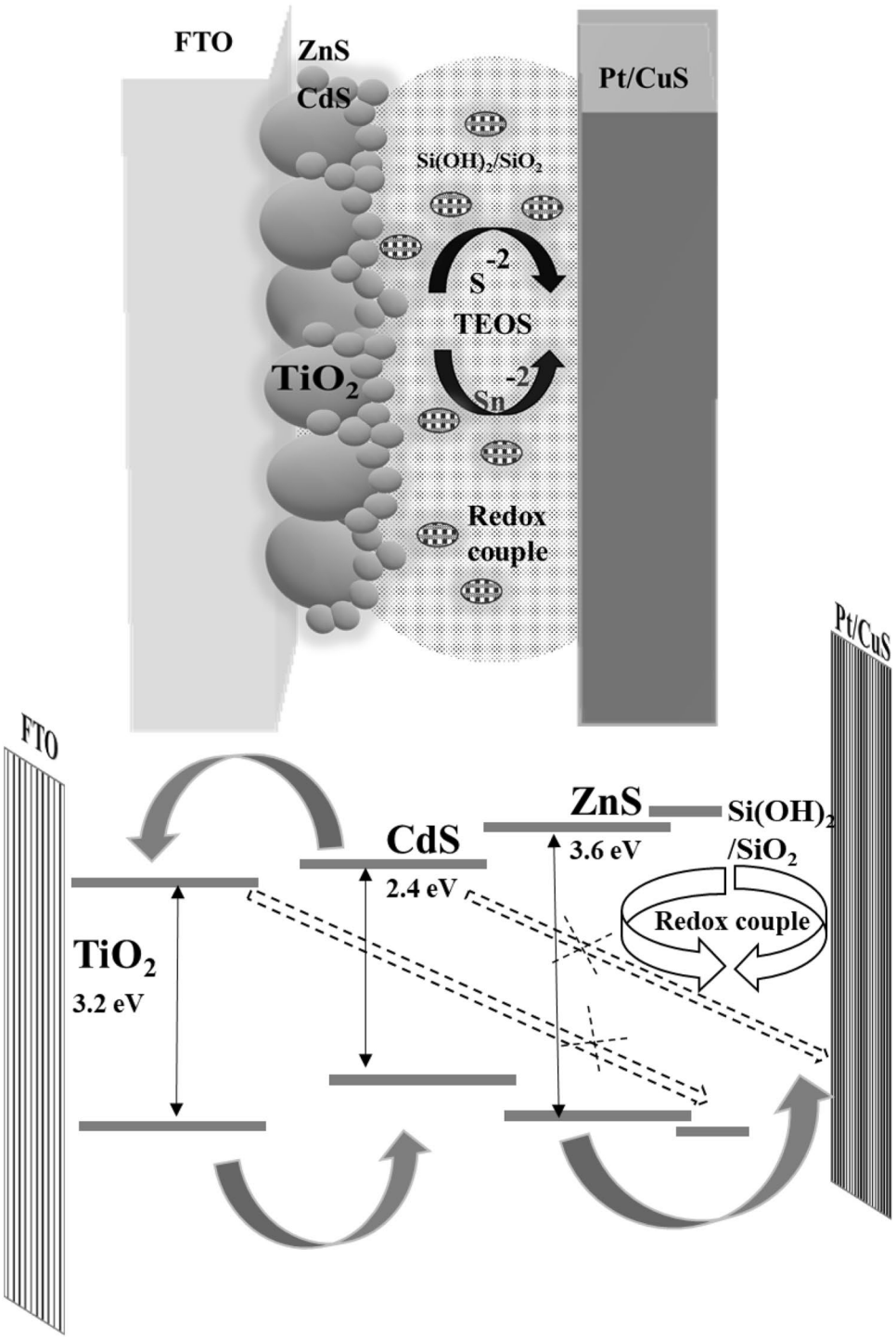

Fig. 10 Schematic diagram for electron transfer mechanism of ZnS passivated CdS-sensitized QDSSC with TEOS additive added polysulphide electrolyte

thereby improve the performance of the cell. When TEOS added into the polysulphide electrolyte solution, it may be transformed into silica or silicon hydroxide by means of hydrolysis reaction in the strong base electrolyte solution [9]. These particles adsorbed on the surface of CdS QDs through the hydroxyl groups and acted as a passivating layer, which suppressed the recombination process [8]. At an optimum concentration of TEOS (2.5 vol%) with polysulphide electrolyte, it supresses back electron transfer and thus enhances overall performance of QDSSC. The

larger diameter of EIS semicircle further confirms the surface passivation of QDs with high R_{ct}. Higher values of Rct obviously rise up a challenging situation for the electrons in the photoanodes to recombine with the holes in electrolyte, leading to a reduced charge recombination. Moreover, the replacement of Pt by CuS CE reduces R_s which results relatively high performance of the QDSSCs [25, 26]. Further the schematic representation of QDSSC configuration with TEOS-modified electrolyte is shown in Fig. 10. The suppression of back electron transfers along with improved passivation resulted from in situ passivation of silica from TEOS additive greatly enhanced the overall cell performance. Therefore, it can be summarized that the QDSSC with TEOS-modified electrolyte and drop-casted CuS CE shows the highest efficiency of 5.5%. The experimental results demonstrated the feasibility of further improvement in PCE of QDSSC by modifying the electrolyte and CE which paves an elegant way for QDSSCs to gain future photovoltaic market.

4 Conclusion

QDSSCs were fabricated by modifying the electrolyte and CEs. The effective loading of QDs onto the TiO_2 photoanodes was confirmed by UV-DRS analysis. The *J–V* characteristics of CdS-based QDSSC with optimum photoanode along with passivating layer were studied by adding different vol% of TEOS into polysulphide electrolyte and the cells with 2.5 vol% of TEOS have shown an improved efficiency of 1.6% with Pt CE. Further, on replacing Pt CE by CuS, the efficiency of QDSSC has improved significantly to 5.5%. The role of TEOS on improving the photovoltaic performance of QDSSC was explored by EIS analysis. The addition of TEOS effectively improves the passivation of QDs thereby suppress the recombination of charge carriers which resulted high efficiency of QDSSCs.

Acknowledgements The author (T.A) is grateful to Department of Science & Technology for financial support (SR/WOS-A/ET-40/2017(G)) under Women Scientists Scheme A(WOS-A). The work is financially supported by DST-SERB under ECR award (ECR/2015/000575) and EMR (EMR/2016/007550).

Declarations

Conflict of interest There is no conflict to declare.

References

1. Nozik AJ, Beard MC, Luther JM, Law M, Ellingson RJ, Johnson JC (2010) Semiconductor quantum dots and quantum dot arrays and applications of multiple exciton generation to third-generation photovoltaic solar cells. Chem Rev 110:6873–6890
2. Guillemoles JF, Kirchartz T, Cahen D, Rau U (2019) Guide for the perplexed to the Shockley–Queisser model for solar cells. Nat Photonics 13:501–505
3. Chebrolu VT, Kim HJ (2019) Recent progress in quantum dot sensitized solar cells: an inclusive review of photoanode, sensitizer, electrolyte, and the counter electrode. J Mater Chem C 7:4911–4933
4. Jeong MS, Son MK, Kim SK, Park S, Prabakar K, Kim HJ (2014) Study on characteristics of CdS quantum dot-sensitized solar cells prepared by successive ionic layer adsorption and reaction with different adsorption times. Electron Mater Lett 10:621–626
5. Jun HK, Careem MA, Arof AK (2013) A suitable polysulfide electrolyte for CdSe quantum dot-sensitized solar cells. Int J Photoenergy. https://doi.org/10.1155/2013/942139
6. Lee YL, Chang CH (2008) Efficient polysulfide electrolyte for CdS quantum dot-sensitized solar cells. J Power Sources 185:584–588
7. Yu Z, Zhang Q, Qin D, Luo Y, Li D, Shen Q, Toyoda T, Meng Q (2010) Highly efficient quasi-solid-state quantum-dot-sensitized solar cell based on hydrogel electrolytes. Electrochem Commun 12:1776–1779
8. Du J, Meng X, Zhao K, Li Y, Zhong X (2015) Performance enhancement of quantum dot sensitized solar cells by adding electrolyte additives. J Mater Chem A 3:17091–17097
9. Yu J, Wang W, Pan Z, Du J, Ren Z, Xue W, Zhong X (2017) Quantum dot sensitized solar cells with efficiency over 12% based on tetraethyl orthosilicate additive in polysulfide electrolyte. J Mater Chem A 5:14124–14133
10. Archana T, Vijayakumar K, Arivanandhan M, Jayavel R (2019) TiO_2 nanostructures with controlled morphology for improved electrical properties of photoanode and quantum dot sensitized solar cell characteristics. Surf Interfaces 17:100350
11. Chen Y, Li Y, Wu C, Wang D, Lin Y, Zhang X, Zou X, Xie T (2020) In-situ preparation of ZnO/$Cu_{2-x}S$ on AZO conductive substrate and applied as counter electrode for quantum dot sensitized solar cells. Sol Energy 207:659–667
12. Duan J, Zhang H, Tang Q, He B, Yu L (2015) Recent advances in critical materials for quantum dot-sensitized solar cells: a review. J Mater Chem A 3:17497–17510
13. Kim HJ, Lee HD, Rao SS, Reddy AE, Kim SK, Thulasi-Varma CV (2016) Well-dispersed NiS nanoparticles grown on a functionalized CoS nanosphere surface as a high-performance counter electrode for quantum dot-sensitized solar cells. RSC Adv 6:29003–29019
14. Thulasi-Varma CV, Gopi CV, Rao SS, Punnoose D, Kim SK, Kim HJ (2015) Time varied morphology controllable fabrication of NiS nanosheets structured thin film and its application as a counter electrode for QDSSC. J Phys Chem 119:11419–11429
15. Wei W, Mi L, Gao Y, Zheng Z, Chen W, Guan X (2014) Partial ion-exchange of nickel-sulfide-derived electrodes for high performance supercapacitors. Chem Mater 26:3418–3426
16. Xu J, Xue H, Yang X, Wei H, Li W, Li Z, Zhang W, Lee CS (2014) Synthesis of honeycomb-like mesoporous pyrite FeS_2 microspheres as efficient counter electrode in quantum dots sensitized solar cells. Small 10:4754–4759
17. Zhu G, Pan L, Sun H, Liu X, Lv T, Lu T, Yang J, Sun Z (2012) Electrophoretic deposition of a reduced graphene–Au nanoparticle composite film as counter electrode for CdS quantum dot-sensitized solar cells. ChemPhysChem 13:769–773
18. Ito S, Chen P, Comte P, Nazeeruddin MK, Liska P, Pechy P, Gratzel M (2007) Fabrication of screen-printing pastes from TiO_2 powders for dye-sensitised solar cells. Prog Photovolt 15:603–612

19. Ito S, Murakami TN, Comte P, Liska P, Gratzel C, Nazeeruddin MK, Gratzel M (2008) Fabrication of thin film dye sensitized solar cells with solar to electric power conversion efficiency over 10%. Thin Solid Films 516:4613–4619
20. Khalili SS, Dehghani H, Afrooz M (2017) Composite films of metal doped CoS/carbon allotropes; efficient electrocatalyst counter electrodes for high performance quantum dot-sensitized solar cells. J Colloid Interface Sci 493:32–41
21. Yeh MH, Lee CP, Chou CY, Lin LY, Wei HY, Chu CW, Vittal R, Ho KC (2011) Conducting polymer-based counter electrode for a quantum-dot-sensitized solar cell (QDSSC) with a polysulfide electrolyte. Electrochim Acta 57:277–284
22. Sankapal BR, Mane RS, Lokhande CD (2000) Deposition of CdS thin films by the successive ionic layer adsorption and reaction (SILAR) method. Mater Res Bull 35:177–184
23. Liu D, Liu J, Liu S, Wang C, Ge Z, Hao X, Du N, Xiao H (2019) The effect of CuS counter electrodes for the CdS/CdSe quantum dot co-sensitized solar cells based on zinc titanium mixed metal oxides. J Mater Sci 54:4884–4892
24. Balis N, Dracopoulos V, Bourikas K, Lianos P (2013) Quantum dot sensitized solar cells based on an optimized combination of ZnS, CdS and CdSe with CoS and CuS counter electrodes. Electrochim Acta 91:246–252
25. Kalanur SS, Chae SY, Joo O (2013) Transparent $Cu_{1.8}S$ and CuS thin films on FTO as efficient counter electrode for quantum dot solar cells. Electrochim Acta 103:91–95
26. Kim HJ, Ko B, Gopi CV, Venkata-Haritha M, Lee YS (2017) Facile synthesis of morphology dependent CuS nanoparticle thin film as a highly efficient counter electrode for quantum dot-sensitized solar cells. J Electroanal Chem 791:95–102
27. Tung HT, Thao NT, Vinh LQ (2018) The reduced recombination and the enhanced lifetime of excited electron in QDSSCs based on different ZnS and SiO_2 passivation. Int J Photoenergy 1:11. https://doi.org/10.1155/2018/8545207
28. Buatong N, Tang IM, Pon-On W (2017) The study of metal sulfide as efficient counter electrodes on the performances of CdS/CdSe/ZnS-co-sensitized hierarchical TiO_2 sphere quantum dot solar cells. Nanoscale Res Let 12:170

Authors and Affiliations

T. Archana[1] · G. Subashini[2] · A. Nirmala Grace[2] · M. Arivanandhan[1] · R. Jayavel[1]

✉ M. Arivanandhan
arivucz@gmail.com

[1] Centre for Nanoscience and Technology, Anna University, Chennai, Tamil Nadu 600025, India

[2] Centre for Nanotechnology Research, Vellore Institute of Technology, Vellore, Tamil Nadu 632014, India